

Shapley Optical Survey. I: Luminosity Functions in the Supercluster Environment*

A. Mercurio¹, P. Merluzzi¹, C. P. Haines¹, A. Gargiulo¹, N. Krusanova¹,
 G. Busarello¹, F. La Barbera¹, M. Capaccioli^{1,2,3}, G. Covone¹

¹ INAF - Osservatorio Astronomico di Capodimonte, via Moiariello 16, I-80131 Napoli, Italy

² Physics Department, Università degli Studi “Federico II”, Napoli, Italy

³ VST Center at Naples (VSTceN), via Moiariello 16, I-80131 Napoli, Italy

Accepted. Received

ABSTRACT

We present the Shapley Optical Survey, a photometric study covering a ~ 2 deg² region of the Shapley Supercluster core at $z \sim 0.05$ in two bands (B and R). The galaxy sample is complete to $B = 22.5$ ($>M^*+6$, $N_{\text{gal}} = 16\,588$), and $R = 22.0$ ($>M^*+7$, $N_{\text{gal}} = 28\,008$). The galaxy luminosity function cannot be described by a single Schechter function due to dips apparent at $B \sim 17.5$ ($M_B \sim -19.3$) and $R \sim 17.0$ ($M_R \sim -19.8$) and the clear upturn in the counts for galaxies fainter than B and R ~ 18 mag. We find, instead, that the sum of a Gaussian and a Schechter function, for bright and faint galaxies respectively, is a suitable representation of the data. We study the effects of the environment on the photometric properties of galaxies, deriving the galaxy luminosity functions in three regions selected according to the local galaxy density, and find a marked luminosity segregation, in the sense that the LF faint-end is different at more than 3σ confidence level in regions with different densities. In addition, the luminosity functions of red and blue galaxy populations show very different behaviours: while red sequence counts are very similar to those obtained for the global galaxy population, the blue galaxy luminosity functions are well described by a single Schechter function and do not vary with the density. Such large environmentally-dependent deviations from a single Schechter function are difficult to produce solely within galaxy merging or suffocation scenarios. Instead the data support the idea that mechanisms related to the cluster environment, such as

* Based on European Southern Observatory Archive Data.

galaxy harassment or ram-pressure stripping, shape the galaxy LFs by terminating star-formation and producing mass loss in galaxies at $\sim M^* + 2$, a magnitude range where blue late-type spirals used to dominate cluster populations, but are now absent.

Key words: Galaxies: clusters: general — Galaxies: clusters: individual: Shapley supercluster — Galaxies: photometry — Galaxies: luminosity function — Galaxies: evolution

1 INTRODUCTION

The properties and evolution of galaxies are strongly dependent on environment (e.g., Blanton et al. 2005; Rines et al. 2005; Smith et al. 2005; Tanaka et al. 2005). In particular the cluster galaxy population has evolved rapidly over the last 4 Gyr (Butcher & Oemler 1984). While distant clusters are dominated, particularly at faint magnitudes, by blue spiral galaxies, often with signs of disturbed morphologies and evidence of multiple recent star-formation events (Dressler et al. 1994), local clusters are completely dominated by passive early-type galaxies.

Recent observational studies on the luminosity, colours, morphology and spectral properties of galaxies have pointed out that the physical mechanisms which produce the transformation in galaxies affecting both the structure and the star formation are naturally driven by and related to the environment (e.g., Treu et al. 2003). These processes are linked in various ways to the local density and the properties of the intra-cluster medium (ICM). In fact, galaxy-ICM interactions, such as ram-pressure stripping and suffocation, require a dense ICM and take place principally in the central cluster regions. The high density regions are also characterized by a steep cluster potential, and we can expect that galaxy-cluster gravitational interactions such as tidal stripping and tidal triggering are also dominant. On the contrary, in low-density environment galaxies have never been through the cluster centre and therefore have never experienced the effects of tidal stripping and tidal triggering of star formation, so the dominant mechanisms are galaxy-galaxy interactions, in terms of both low-speed interactions between galaxies of similar mass (mergers) and high-speed interactions between galaxies in the potential of the cluster (harassment).

The above mentioned mechanisms affect differently the observed morphology and/or the star formation properties of galaxies. In particular, galaxy harassment and ram pressure stripping cause a partial loss of gas mass and, depending on the fraction of gas removed and its rate, ram-pressure stripping can lead either to a rapid quenching of star formation or to a slow decrease in the star formation rate (Larson, Tinsley, & Caldwell 1980; Balogh et al. 2000; Diaferio et al. 2001; Drake

et al. 2000). Successive high-speed encounters between galaxies (galaxy harassment) lead to gas inflow and strong star formation activity (Fujita 1998).

With the aim to investigate the effects of the environment on the galaxy population, we have undertaken an optical study of the Shapley Supercluster (SSC) core, one of the densest structures in the nearby Universe. The study of this region, selected because of its physical peculiarity in terms of density and complexity, but also for the availability of multiwavelength observations, will take advantage of deep optical photometry from the ESO Archive covering an area of 2 deg². The Shapley Optical Survey (SOS) in B and R bands provides a galaxy sample complete and reliable up to 22.5 mag and 22.0 mag in B and R bands, respectively. We plan to use the excellent SOS dataset to study, with respect to the supercluster environment, the distribution of galaxy populations both in luminosity and colour and the galaxy structural properties comparing the observations with theoretical predictions. In the present paper we will present the dataset, the catalogues and the galaxy luminosity functions in B and R bands as function of the SSC environment.

The galaxy luminosity function (LF), which describes the number of galaxies per unit volume as function of luminosity, is a powerful tool to constrain galaxy transformations, since it is directly related to the galaxy mass function. Moreover, the effect of environment on the observed galaxy LF could provide a powerful discriminator among the proposed mechanisms for the transformations of galaxies. The effects of galaxy merging and suffocation on the cluster galaxy population have been studied through combining high-resolution N-body simulations with semi-analytic models for galaxy evolution (e.g., Springel et al. 2001; Kang et al. 2005). These show that while galaxy merging is important for producing the most luminous cluster galaxies, the resultant LF can always be well described by a Schechter (Schechter 1976) function, although both M^* and the faint-end slope can show mild trends with environment. Galaxy mergers are also inhibited once the relative encounter velocities become much greater than the internal velocity dispersion of galaxies, and so are rare in rich clusters (Ghigna et al. 1998). In contrast, galaxy harassment and ram-pressure stripping may change the LF shape as galaxies lose mass in interactions with other galaxies, the cluster's tidal field, and the ICM. In particular Moore, Lake & Katz (1998) showed that harassment has virtually no effect on a system as dense as a giant elliptical galaxy or a spiral bulge and only purely disk galaxies can be turned into spheroidals, so these mechanisms produce a cutoff for Sd-Im galaxies. Since the luminosity function is strongly type specific, and those for Sc and Sd/Im galaxies can be described by narrow ($\sigma \sim 1$ mag) Gaussian distributions centred at $\sim M^* + 1$ and $\sim M^* + 3$ (de Lapparent 2003), the effects of galaxy harassment could be characterized by a dip in the LF at these magnitudes.

In order to further investigate and to assess the relative importance of the processes that may be responsible for the galaxy transformations, we have performed a photometric study of the SSC core, examining in particular the effect of the environment through the comparison of luminosity functions in regions with different local densities.

The SSC was observed by Raychaudhury (1989) and the LF was firstly derived by Metcalfe, Godwin & Peach (1994; hereafter MGP94). By using photographic data, they investigate a region of 4.69 deg^2 around the cluster A 3558 considering a sample of 4599 galaxies complete and uncontaminated by stars (to 2% level) for $b < 19.5$. The derived LF for the central region of 1.35 deg^2 showed a broad peak in the number of galaxies at $b = 18$ which cannot be well fitted by a Schechter function. Moreover, MGP94 found a deficit of blue galaxies in the A 3558 core suggesting morphological segregation. However, their study is limited to bright magnitudes, preventing the determination of the faint-end slope while taking advantage of deeper photometry and larger sample of galaxies distributed in larger SSC area, we can provide clear evidence on the LF shape thus quantifying the environmental effect on the LF properties.

The layout of this work is the following. General information of the structure of the SSC core are summarized in Sect. 2. We describe observations, data reduction and the photometric calibrations in Sect. 3. The catalogues are presented in Sect. 4. Sect. 5 is dedicated to the definition of the environment and in Sect. 6 we show the LFs. Finally Sect. 7 contains the summary and the discussion of the results. In this work we assume $H_0 = 70 \text{ km s}^{-1} \text{ Mpc}^{-1}$, $\Omega_m = 0.3$, $\Omega_\Lambda = 0.7$. According to this cosmology, 1 arcmin corresponds to 0.060 Mpc at $z = 0.048$.

2 THE SHAPLEY SUPERCLUSTER

The SSC represents an ideal target for the investigation of the role played by environment in the transformation of galaxies, and has been investigated by numerous authors since its discovery (Shapley 1930). It is one of the richest supercluster in the nearby universe, consisting of as many as 25 Abell clusters in the redshift range $0.035 < z < 0.055$. Extensive redshift surveys (Bardelli et al. 2000; Quintana, Carrasco & Reisenegger 2000; Drinkwater et al. 2004) indicate that these clusters are embedded in two sheets extending over a $\sim 10 \times 20 \text{ deg}^2$ region of sky ($\sim 35 \times 70 h_{70}^{-2} \text{ Mpc}^2$), and that as many as half the total galaxies in the supercluster are from the inter-cluster regions. The Shapley core (Fig. 3) is constituted by three Abell clusters: A 3558 ($z=0.048$, Melnick & Quintana 1981; Metcalfe, Godwin & Spenser 1987; Abell richness $R=4$, Abell, Corwin & Olowin 1989), A 3562 ($z=0.049$, Struble & Rood 1999, $R=2$, Abell et al. 1989) and A 3556

($z=0.0479$, Struble & Rood 1999, $R=0$, Abell et al. 1989) and two poor clusters SC 1327-312 and SC 1329-313. Dynamical analysis indicates that at least a region of radius $11 h_{70}^{-1} \text{Mpc}$ centred on the central cluster A 3558, and possibly the entire supercluster, is past turnaround and is collapsing (Reisenegger et al. 2000), while the core complex itself is in the final stages of collapse, with infall velocities reaching $\sim 2000 \text{ km s}^{-1}$.

A major study of the dynamical properties of the supercluster core was performed by Bardelli et al. (2001 and reference therein). They showed that the supercluster core has a complex, highly elongated structure, and identified 21 significant 3-dimensional subclumps, including eight in the A 3558 cluster alone.

The X-ray observations show that the supercluster has a flattened and elongated morphology where clusters outside the dense core are preferentially located in hot gas filaments (Bardelli, Zucca, & Malizia 1996; Kull & Böhringer 1999; De Filippis, Schindler & Erben 2005). Moreover, Finoguenov et al. (2004) showed a strong interaction between the cluster A 3562 and the nearby group SC 1329-313 with an associated radio emission having young age (Venturi et al. 2000, 2003). However, since this is one of the weakest radio halos found, Venturi et al. (2003) suggested that this halo is connected with the head-on radio galaxy of A 3562. Bardelli et al. (2001) suggested that the A 3558 complex is undergoing a strong dynamical evolution through major merging seen just after the first core-core encounter, and so the merging event has already been able to induce modifications in the galaxy properties. Very recently, Miller (2005), with a radio survey of a 7 deg^2 region of SSC, found a dramatic increase in the probability for galaxies in the vicinity of A 3562 and SC 1329-313 to be associated with radio emission. He interpreted this fact as a young starburst related to the recent merger of SC 1329-31 with A 3562.

3 OBSERVATIONS, DATA REDUCTION AND PHOTOMETRIC CALIBRATION

The SOS data obtained from the ESO Archive (68.A-0084, P.I. Slezak), were acquired with the ESO/MPI 2.2-m telescope at La Silla. We analysed B- and R-band photometry of eight contiguous fields covering a 2 deg^2 region centred on the SSC, as shown in Fig. 1.

The observations (see Table 1 for details) were carried out with the WFI camera, a mosaic of eight 2046×4098 pixels CCDs, mounted on the Cassegrain focus of the telescope. The camera has a field of view of $34' \times 33'$, corresponding to $2.0 \times 1.9 h_{70}^{-2} \text{ Mpc}^2$ at the cluster redshift, and a pixel scale of 0.238 arcsec. The total exposure times for each field are 1500 s (300 s \times 5) in B band and 1200 s (240 s \times 5) in R band, reaching the $R=25$ ($B=25.5$) at 5σ . The single exposures

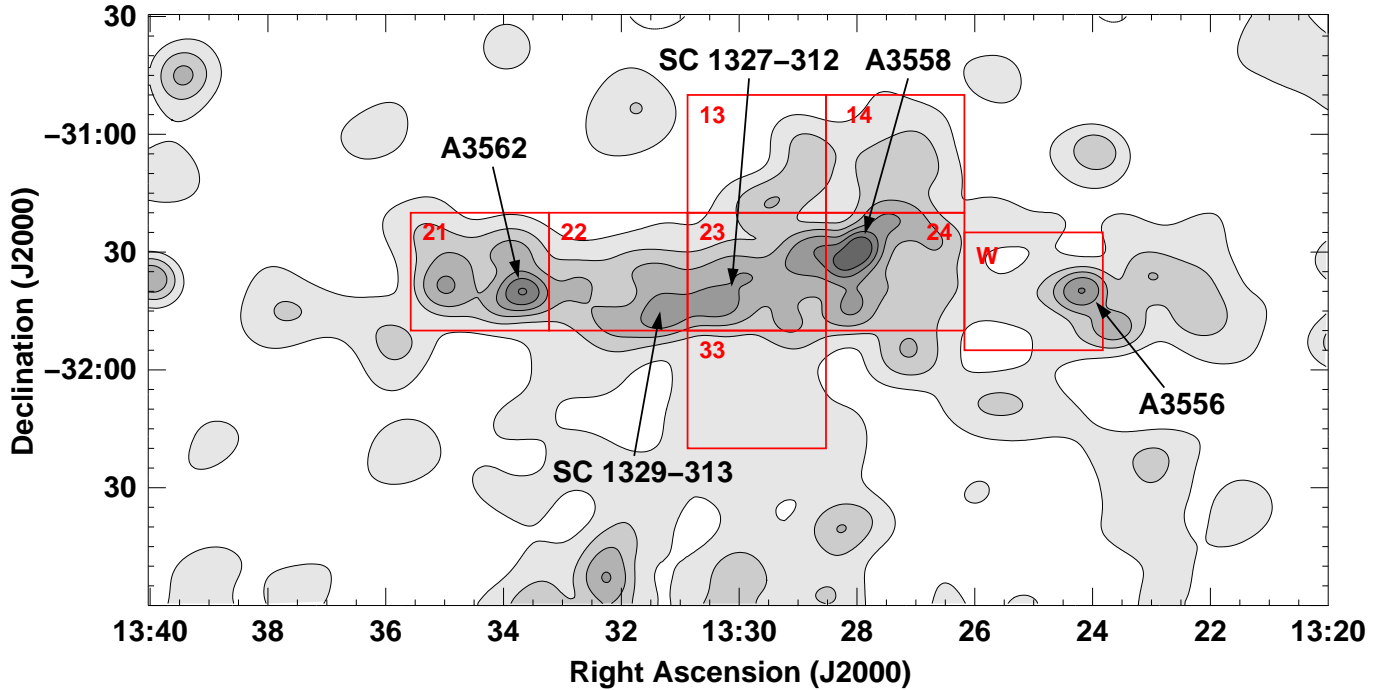


Figure 1. The surface density of $R < 18.5$ galaxies of the the SSC core, obtained by using data of the SuperCosmos Sky Survey (Hambly, MacGillivray & Read 2001). Red rectangles indicate the 8 analysed fields in SOS.

Table 1. The observations.

Field #	Band	Centre RA, Dec	Date	FWHM arcsec
21	B	13:34:24.1, -31:34:57.1	18 March 2002	0.95
	R	13:34:24.1, -31:34:57.0	"	0.87
22	B	13:32:03.2, -31:34:57.1	18 March 2002	0.79
	R	13:32:03.2, -31:34:57.1	"	0.70
23	B	13:29:42.4, -31:34:57.3	18 March 2002	0.76
	R	13:29:42.4, -31:34:57.5	"	0.71
24	B	13:27:21.5, -31:34:57.4	18 March 2002	0.77
	R	13:27:21.5, -31:34:57.1	"	0.73
W	B	13:25:00.6, -31:40:27.1	18 March 2002	0.83
	R	13:25:00.6, -31:40:26.6	"	0.73
13	B	13:29:42.5, -31:04:58.0	9 April 2003	0.98
	R	13:29:42.5, -31:04:59.3	9 June 2002	1.11
14	B	13:27:21.6, -31:04:57.6	19 March 2002	1.16
	R	13:27:21.5, -31:04:56.6	"	1.27
33	B	13:29:42.4, -32:04:57.5	9 April 2003	0.81
	R	13:29:42.3, -32:04:58.9	9 June 2002	1.43

are jittered to cover the gaps between the different CCDs of the camera. Landolt (1992) stars were observed in order to perform accurate photometric calibration.

We used the ALAMBIC pipeline (version 1.0, Vandame 2004) to reduce and combine the SOS images. The pipeline follows the standard procedures for bias subtraction and flat-field correction; the twilight sky exposures for each band were used to create the master flat.

The photometric calibration was performed into the Johnson-Kron-Cousins photometric sys-

Table 2. The results of the photometric fit for B and R band.

Observing Night	Band	<i>C</i>	<i>ZP</i>	<i>A</i>	γ	rms
18 March 2002	B	B - R	-24.531 ± 0.024	0.189 ± 0.017	-0.131 ± 0.009	0.041
18 March 2002	R	V - R	-24.548 ± 0.038	0.147 ± 0.026	0.049 ± 0.035	0.036
9 April 2003	B	B - R	-24.562 ± 0.029	0.162 ± 0.019	-0.141 ± 0.017	0.034

tem using the Landolt stars. With the IRAF tasks DAOPHOT and APPHOT we computed the instrumental magnitude of the stars in a fixed aperture in B and R bands.

For the R band we calibrated the flux by adopting the following relation:

$$M' = M + \gamma C + AX + ZP, \quad (1)$$

where M is the magnitude of the star in the standard system, M' is the instrumental magnitude, γ is the coefficient of the colour term, C is the colour of the star in the standard system, A is the extinction coefficient, X is the airmass and ZP is the zero point. For the B band we took into account the colour term (B-R). The results are reported in Table 2.

Since photometric standards were not available for the nights of 9 June 2002 and 19 March 2002, we adopted relative calibration for fields #13, #33 in R band and field #14 both in B and R band. The photometric accuracy for the zero point was about 0.04 mag in both bands.

4 THE CATALOGUES

The photometric catalogues from the SOS images were produced using SExtractor (Bertin & Arnouts, 1996) together with a set of software procedures developed by the authors in order to increase the quality of final catalogues, avoiding spurious detections and misleading results (see Sect. 4.1).

The star/galaxy classification was based on both the parameter *class star* (CS) of SExtractor and the value of the *full width at half maximum* (FWHM). Stars were defined as those objects with $CS \geq 0.98$ or having FWHM equal to those of bright, non saturated stellar sources in the image.

The completeness magnitudes were firstly estimated using the prescription of Garilli et al. (1999). Then the reliability and the completeness of the catalogues were checked performing MonteCarlo simulations by adding artificial stars and galaxies (see Sect. 4.2). The final catalogues consist of 16 588 and 28 008 galaxies in B and R band, respectively, up to the completeness magnitude limits B=22.5 and R=22.0.

Aperture and Kron (Kron 1980) magnitudes were measured in each band. For aperture pho-

tometry we referred to the aperture of 17 arcsec (~ 8 kpc) of diameter used by Bower, Lucey and Ellis (1992) for Coma. Converting this value from Coma redshift to our redshift we used an aperture of 8 arcsec of diameter. Kron magnitudes (M_{Kron}) were computed in an adaptive aperture with diameter $a \cdot R_{Kron}$, where R_{Kron} is the Kron radius and a is a constant. We chose $a = 2.5$, yielding $\sim 94\%$ of the total source flux within the adaptive aperture (Bertin & Arnouts 1996). We measured the Kron magnitude for all the objects in the catalogues without applying any correction to the total magnitude. The uncertainties on the magnitudes were obtained by adding in quadrature both the uncertainties estimated by SExtractor and the uncertainties on the photometric calibrations. The measured magnitudes were corrected for galactic extinction ($B=0.238$ and $R=0.149$) following Schlegel, Finkbeiner & Davis (1998). Luminosity functions were computed by means of Kron magnitudes, while aperture magnitudes were used for measuring galaxy colours. SOS catalogues are available on request.

4.1 Cleaning procedure

In order to obtain *clean* catalogues we used the following approach that takes into account both the performances of SExtractor and the characteristics of the analysed fields (crowdness, background fluctuations, bright objects sizes and distribution).

We ran SExtractor with two different deblending parameters. We produced the bulk of the catalogue adopting a low deblending parameter (0.0001), which allows a suitable detection of close objects. Then we corrected the multiple detections of bright extended objects using a high deblending parameter (>0.01).

The combined images show a significant number of bad and warm pixels, and cosmic rays residuals often detected by SExtractor as sources. These spurious detections were identified and then removed since either they are present only in few exposures or they are particularly compact, comparing their M_{Kron} with the magnitude measured over the central pixel.

In the vicinity of bright galaxies with extended halos, SExtractor sometimes overestimates R_{Kron} and M_{Kron} . These objects were identified and their M_{Kron} corrected.

Finally, we removed spurious objects, ghosts or diffraction spikes around bright ($R<15$) stars by defining circular avoidance regions (whose area is proportional to the stars flux level).

Table 3. Completeness and reliability of the SOS catalogues

R	completeness		% of stars
	mag	missclassified	
20.0–20.5	98.4	2.1	
20.5–21.0	97.3	3.0	
21.0–21.5	95.3	4.1	
21.5–22.0	94.3	8.0	
22.0–22.5	92.0	34.8	
22.5–23.0	88.1	75.6	

4.2 Completeness and reliability

The first estimates of the completeness magnitudes, derived using the prescription of Garilli et al. (1999), are 23.0 in the R band, and 23.5 in the B band. We checked the reliability and completeness of the SOS catalogues for each 0.5 magnitude bin by adding 10 000 artificial stars and galaxies to the images, and computing the fraction of these sources detected and correctly classified by SExtractor. The artificial stars were created by taking a bright, non-saturated star ($R \sim 17$) in the image and dimming it to the appropriate magnitude, while the galaxies were simulated by taking galaxies of differing Hubble types and the appropriate magnitude from the Hubble Ultra Deep Field (using photometry from the COMBO-17 Chandra Deep Field South catalogue; Wolf et al. 2004), resampling them to the resolution of the WFI, and convolving them with the image Point Spread Function (PSF).

At $R = 22.0$, 94.3% of the simulated galaxies were successfully detected and classified. In the SOS field the number of stars and galaxies become equal at $R = 21.4$. Beyond $R = 22.0$ the fraction of stars misclassified as galaxies increases dramatically mainly due to the blending of the sources. Moreover, further stellar contamination is due to the high number density of both stars and galaxies in this field (the Galactic latitude of the field is $+30^\circ$) which increases the frequency of star-star and star-galaxy blends that can be misclassified as single galaxies. The estimates of completeness and reliability for the R band are shown in Table 3. Analogous results were obtained for the B band.

We adopted the conservative limits $R = 22.0$ and $B = 22.5$ as the magnitudes below which stellar contamination can be modelled and accounted for in the galaxy LF determination.

5 QUANTIFYING THE GALAXY ENVIRONMENT

To study the effect of the environment on galaxies in the SSC core, the local density of galaxies, Σ , was determined across the WFI mosaic. This was achieved using an adaptive kernel estima-

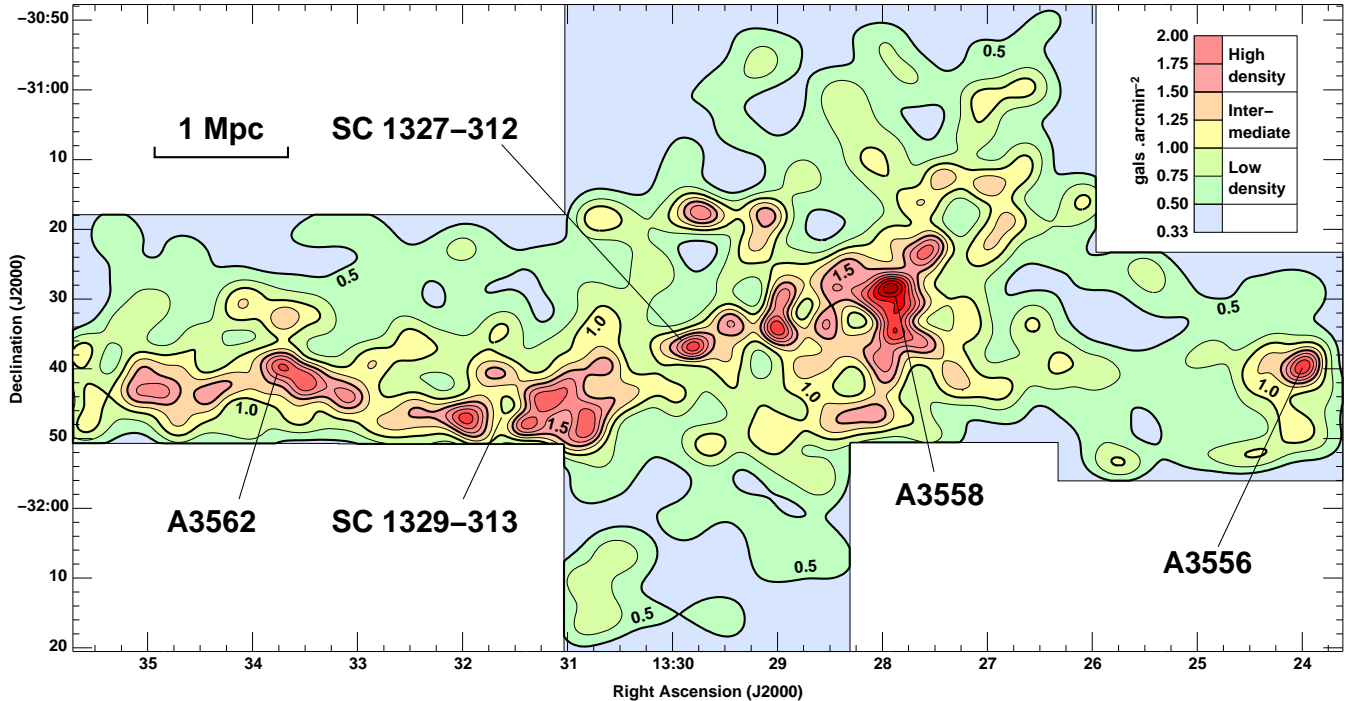


Figure 2. The surface density of $R < 21.0$ galaxies in the region of the SSC core complex. Isodensity contours are shown at intervals of 0.25 galaxies arcmin^{-2} , with the thick contours corresponding to 0.5, 1.0 and 1.5 galaxies arcmin^{-2} , the densities used to separate the three cluster environments. The area corresponds to $9.0 \times 5.4 h_{70}^{-2} \text{ Mpc}^2$ at $z=0.048$.

tor (Pisani 1993; 1996), in which each galaxy i is represented by a Gaussian kernel, $K(r_i) \propto \exp(-r^2/2\sigma_i^2)$, whose width σ_i is proportional to $\Sigma_i^{-1/2}$ thus matching the resolution locally to the density of information available. For this study, we considered the surface number density of $R < 21.0$ ($< M^* + 6$) galaxies, with an additional colour cut applied to reject those galaxies more than 0.2 mag redder in B-R than the observed red sequence (Eq. 2) to minimize background contamination. As there are no known structures in the foreground of the SSC core (90% of $R < 16$ galaxies have redshifts confirming that they belong to the supercluster), any substructure identified in the density map is likely to be real and belonging to the supercluster. The local density was initially determined using a fixed Gaussian kernel of width 2 arcmin, and then iteratively recalculated using adaptive kernels. The resultant surface density map of the SSC core complex is shown in Fig. 2, with the three clusters and two groups indicated. Isodensity contours are shown at intervals of 0.25 galaxies arcmin^{-2} , with the thick contours corresponding to 0.5, 1.0 and 1.5 galaxies arcmin^{-2} , the densities used to separate the three supercluster environments described below. The background density of galaxies as estimated from an area of 5 deg^2 of the Deep Lens Survey (DLS, Wittman et al. 2002) is 0.335 galaxies arcmin^{-2} , and hence the thick contours correspond to overdensity levels of ~ 50 , 200 and 400 galaxies $h_{70}^2 \text{ Mpc}^{-2}$ respectively. The entire region covered by the SOS is overdense with respect to field galaxy counts.

Table 4. Fits to the LFs. Errors on the M^* and α parameters can be obtained from the confidence contours shown in Figs. 3, 8 and 9. In the table S indicates the fit with a single Schechter and G+S those with Gaussian plus Schechter.

Region	Band	Function	m^*	M^*	α	μ	σ	χ^2_v	$P(\chi^2 > \chi^2_v)$
all field	B	S	15.35	-21.42	-1.46			2.62	0.08%
all field	B	G + S	15.53	-21.24	-1.74	17.01	-19.76	1.32	0.36 97.1%
high density	B	S	14.64	-22.13	-1.46			0.95	50.3%
high density	B	G + S	16.47	-20.32	-1.51	17.00	-19.77	1.73	0.94 50.0%
int density	B	S	15.01	-21.76	-1.50			1.33	18.6%
int density	B	G + S	15.46	-21.31	-1.56	16.51	-20.26	0.85	0.50 89.1%
low density	B	S	15.57	-21.20	-1.49			2.22	0.69%
low density	B	G + S	16.11	-20.66	-1.66	16.96	-19.81	1.09	0.60 81.5%
all field	R	S	14.52	-22.26	-1.26			1.23	23.5%
all field	R	G + S	13.72	-23.06	-1.62	15.89	-20.89	1.23	0.46 94.7%
high density	R	S	14.29	-22.49	-1.30			0.86	61.7%
high density	R	G + S	14.15	-22.63	-1.30	20.92	-15.86	3.15	1.01 43.8%
int density	R	S	14.27	-22.51	-1.39			1.28	20.5%
int density	R	G + S	15.00	-21.78	-1.43	15.22	-21.49	0.98	0.74 71.3%
low density	R	S	13.75	-23.03	-1.50			3.33	0.002%
low density	R	G + S	15.28	-21.50	-1.80	16.37	-20.41	1.58	1.25 24.7%

6 SOS LUMINOSITY FUNCTIONS

The LF in each band in the whole surveyed area was obtained up to the completeness magnitude limits, removing the interlopers by statistically subtracting the background contamination, as determined from thirteen control fields of the DLS, covering a total area of $\sim 4.4 \text{ deg}^2$. The adopted procedures for background subtraction are explained in Sect. 6.1.

In order to investigate the effects of the environments we derived and compared the LFs, determined in the three different regions characterized by high-, intermediate- and low-densities of galaxies.

We fitted the observed galaxy counts with a single Schechter (S) function. However, since the LFs were generally poorly fitted by using such a model, the fits were also computed with the sum of Gaussian and Schechter (G+S) functions (Sect. 6.2 and Sect. 6.3) in order to describe bright and faint galaxy populations (e.g., de Lapparent et al. 2003; Molinari et al. 1998; Biviano et al. 1995). Moreover, we compared the LFs with the counts of the red sequence galaxies (Sect. 6.4). We selected also galaxies bluer than the colour magnitude relation in order to derive the luminosity function of late-type galaxy populations.

Absolute magnitudes were determined using the k-corrections for early-type galaxies from models of Bruzual & Charlot (2003). All the fit parameters and associated χ^2 statistics are listed in Table 4.

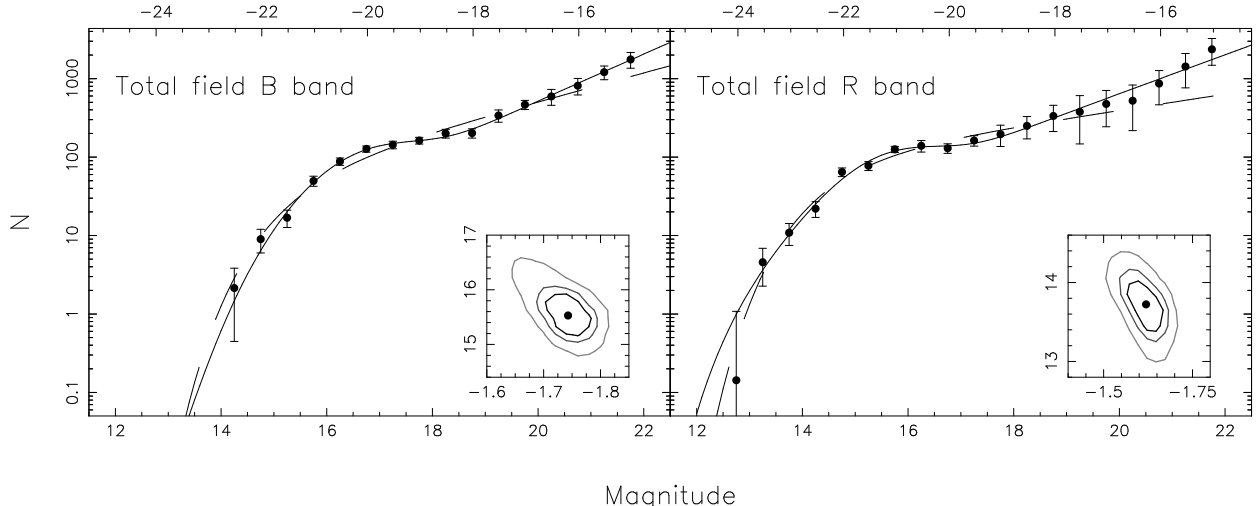


Figure 3. Luminosity function in the B and R bands over 2 deg^2 field covering the core of the SSC. Dashed and continuous lines are fits with the S and with the G+S functions (see text), respectively. In the small panels the 1, 2 and 3σ confidence levels of the best-fit parameters for α and M^* from the G+S fit, are shown. The counts are per half magnitudes.

6.1 Background galaxy subtraction

Since the region covered by the SOS lies completely within the overdensity corresponding to the core complex, to perform a reliable statistical subtraction of field galaxies a suitable large control field is required, that has been observed with a similar filter set (B and R) to at least the depth of the SOS. The large area is necessary in order to minimize the effects of cosmic variance and small number statistics.

To this aim we chose the DLS, which consists of deep BVRz' imaging of seven $2^\circ \times 2^\circ$ degree fields. The observations have been made using the Mosaic-II cameras on the NOAO KPNO and CTIO 4-m telescopes, with exposure times of 12 000 s in BVRz' and 18 000 s in R, resulting in 5σ depths of $B, V, R \sim 27$. The R-band images were obtained in good seeing conditions with a FWHM of $0.9''$ whereas the other bands have FWHM around $1.2''$.

The catalogues were extracted following the same procedures of the SOS data. We considered thirteen $35' \times 35'$ Mosaic-II fields, covering a total area of ~ 4.44 square degrees (after removal of regions around bright stars) in two well separated regions of sky (fields 2 and 4 in the DLS). Given the depth of the DLS images, star-galaxy separation using the combined stellarity-FWHM classification method was found to be $>99\%$ efficient to $R = 22.0$. There are no nearby clusters in the regions covered. The rich cluster A 0781 at $z = 0.298$ is however located within field 2, and so the two affected fields closest to the centre of the cluster were not included among the thirteen.

We used data from the thirteen control fields to estimate the background counts and the fluctuation amplitude as in Bernstein et al. (1995). In this case the background counts were estimated as the mean of the control field counts (Eq. 1 Bernstein et al. 1995), and the fluctuations as the rms

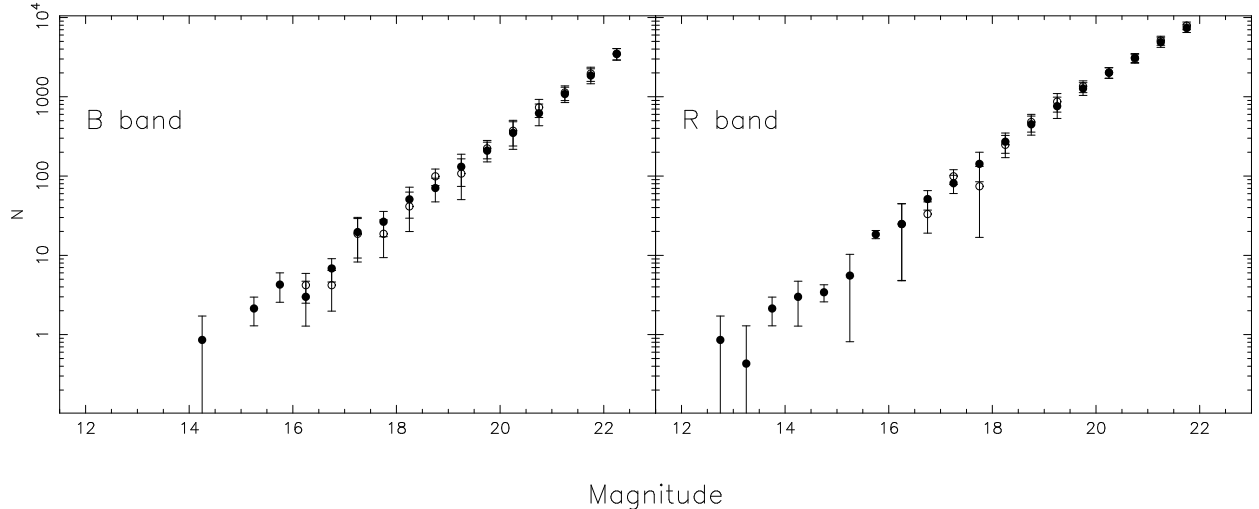


Figure 4. Comparison of galaxy counts obtained from the DLS (filled circles) and ESO-Sculptur Survey (open circles). The counts are normalized to the total area covered by the SOS data and are per half magnitude.

of the counts in each control field respect to the mean estimated in the all area (Eq. 2 Bernstein et al. 1995).

The galaxy number-magnitude counts obtained from the DLS data were found to be consistent with those from the literature (e.g., Arnouts et al. 1997) for the same passbands (see Fig. 4). An estimate for the total effect from the cosmic variance from the fluctuations of galaxy counts among the thirteen fields confirmed that, when combined, the obtained number magnitude counts are robust against cosmic variance.

The counts of SSC galaxies were defined as the difference between the counts detected in the supercluster fields and those estimated for the background (Eq. 3 Bernstein et al. 1995). By considering this definition, the uncertainties were measured as the sum in quadrature of fluctuation in the background and in the supercluster counts (Eq. 4 Bernstein et al. 1995).

In order to avoid the background counts taken from the DLS being too low, we make an additional comparison between SOS and DLS data. We selected galaxies 3σ redder than the observed red sequence (Eq. 2 and Eq. 3) in the SOS. Since galaxies redward of the sequence should be almost all background galaxies we compared these counts with those obtained for the DLS control fields applying the same colour cut. Figure 5 shows that these counts are consistent.

6.2 The total luminosity functions

Figure 3 shows the LFs in B and R bands for galaxies over the whole 2 deg^2 SOS area, covering the SSC core (Fig. 1). The parameters of the fit are reported in Table 4. The weighted parametric fit of a S function (dashed lines in Fig. 3) is unable to describe the observed changes in slope of the LF

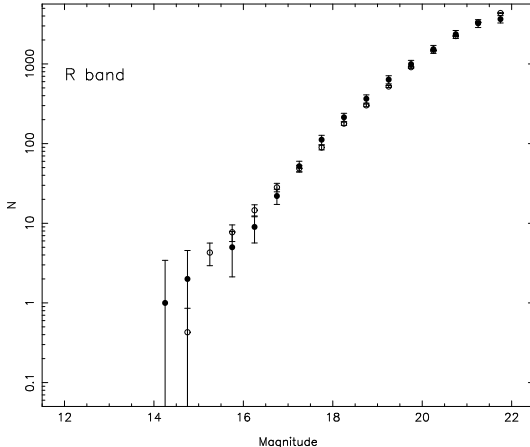


Figure 5. Comparison of R-band counts for galaxies redder than the red sequence (see text) obtained from the SSC (filled circles) and the DLS (open circles). The counts are normalized to the total area covered by the SOS data and are per half magnitude.

at faint magnitudes, in particular the dips apparent at $B \sim 17.5$ ($M_B \sim -19.3$) and $R \sim 17.0$ ($M_R \sim -19.8$) and the clear upturn in the counts for galaxies fainter than B and $R \sim 18$ mag, apparent in Fig. 3. To successfully model these changes in slope requires a composite G+S LF (continuous line, Fig. 3), which represent the data distribution significantly better in both B ($P(\chi^2 > \chi^2_v) = 97\%$ against $P(\chi^2 > \chi^2_v) = 0.08\%$) and R bands ($P(\chi^2 > \chi^2_v) = 95\%$ against $P(\chi^2 > \chi^2_v) = 23\%$). The S function fails most dramatically to describe the upturn in the galaxy counts at faint magnitudes, as demonstrated by the composite R-band faint-end slope being -1.62 as opposed to the S slope of -1.26 .

An upper limit to the background counts could be set by using the counts for galaxies in the SOS region with density less than 0.5, covering an area of $\sim 0.5 \text{ deg}^2$. The obtained LFs are consistent with those obtained by using DLS counts, but the error bars are too large to make any definitive conclusion on the faint-end part of the luminosity function.

6.3 The effect of environment

Figures 6 and 7 show the B- and R-band galaxy LFs in the high-, intermediate- and low-density regions, covering areas of ~ 0.118 , ~ 0.344 , $\sim 1.125 \text{ deg}^2$, respectively. Each LF was modelled by a weighted parametric fit to S (dashed lines) and to composite G+S functions (continuous lines). The best-fit values are listed in Table 4.

According to the χ^2 statistics in both bands the fit with a S function can be rejected in the low-density region, the LFs showing a bimodal behaviour due to the presence of a dip and an upturn for faint galaxies, that cannot be fitted by using a single function. In the intermediate-density region, although the S function cannot be rejected, its fit gives a worse representation of the global

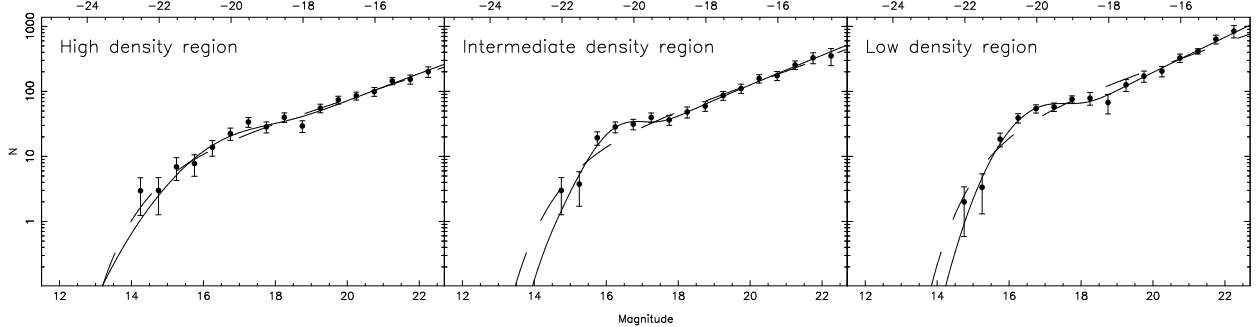


Figure 6. The B-band LFs of galaxies in the three cluster regions corresponding to high-, intermediate- and low-density environments. Dashed and continuous lines represent the fit with a S and a G+S respectively. The counts are per half magnitudes.

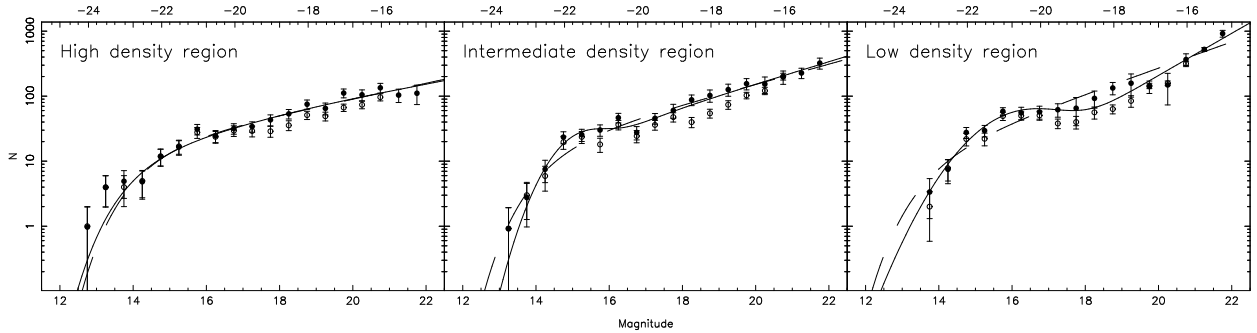


Figure 7. The R-band LFs of galaxies in the three regions corresponding to high-, intermediate- and low-density environments. Filled circles represent counts obtained from the photometric catalogue with a statistical background subtraction, open circles are the counts of galaxies with $R < 21$ belonging to the red sequence of the CM relation (see Sect. 6.3). Dashed and continuous lines represent the fit with a S and a G+S function respectively. The counts are per half magnitudes.

distribution of data compared with a composite function ($P(\chi^2 > \chi^2_\nu) \sim 20\%$ against $P(\chi^2 > \chi^2_\nu) \sim 70\text{--}80\%$). On the other hand, in the high-density region the fit with a S function is more suitable.

Figures 8 and 9 show the confidence contours of the best fitting functions for B and R band, respectively, for the three density regions. The faint-end slope becomes significantly steeper from high- to low-density environments varying from -1.46 to -1.66 in B and from -1.30 to -1.80 in R band, being inconsistent at more than 3σ confidence level (c.l.) in both bands (right panel

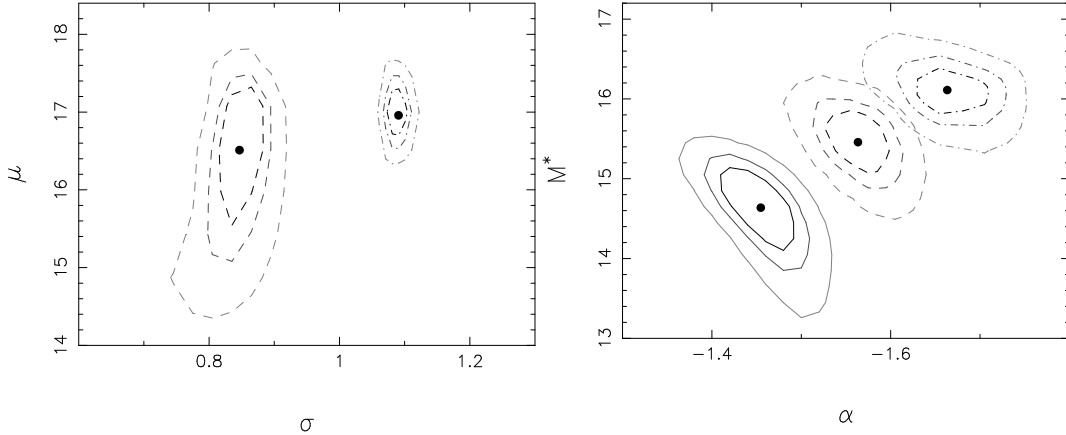


Figure 8. The 1, 2 and 3σ confidence levels for the B-band best-fitting Gaussian (left panel) and Schechter (right panel) parameters for the three cluster regions corresponding to high- (solid contours), intermediate- (dashed) and low-density (dot-dashed) environments. Contours in the high-density region are obtained by fitting data with a S function.

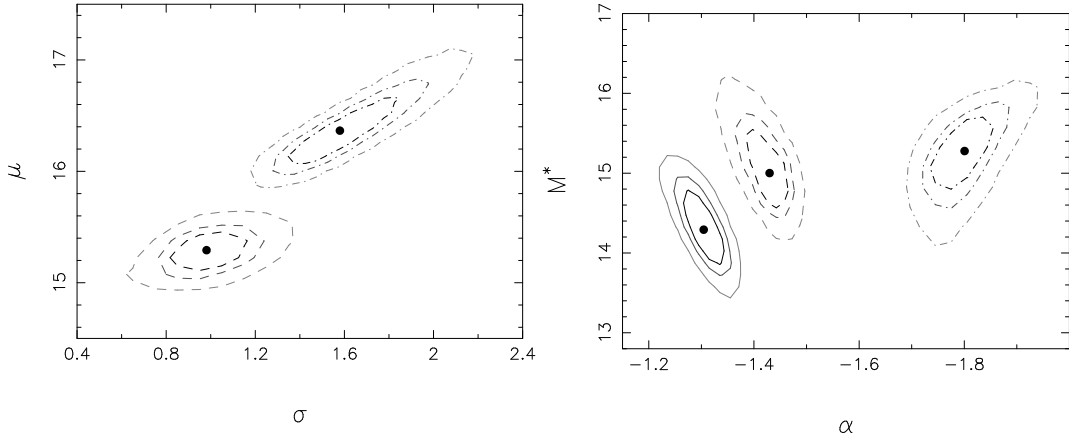


Figure 9. The 1, 2 and 3σ confidence levels for the R-band best-fitting Gaussian (left panel) and Schechter parameters (right panel) for the three cluster regions corresponding to high- (solid contours), intermediate- (dashed) and low-density (dot-dashed) environments. Contours in the high-density region are obtained by fitting data with a S function.

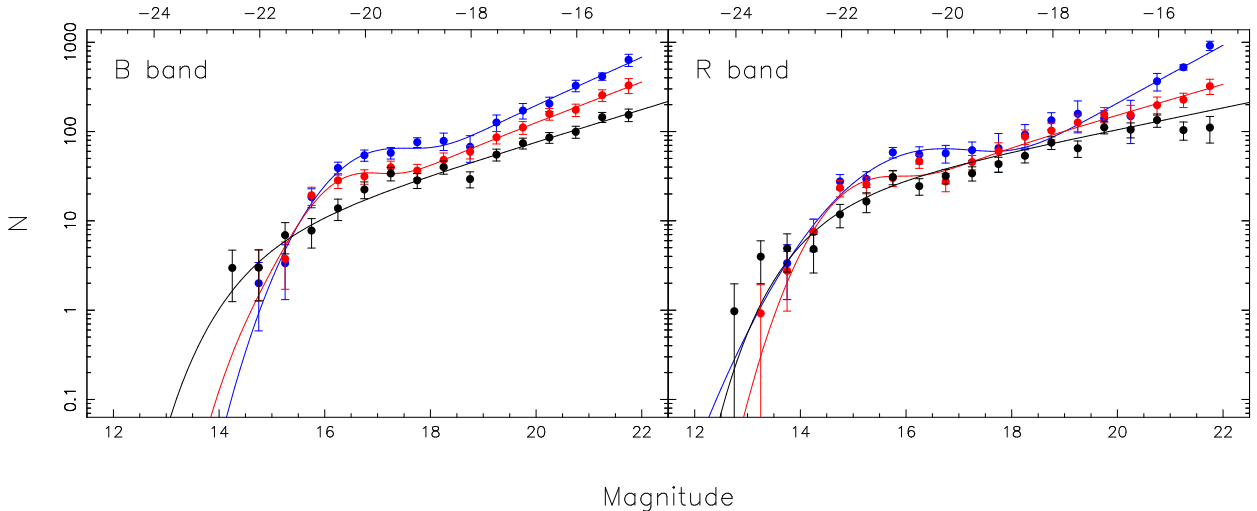


Figure 10. The B- (left panel) and R-band (right panel) LFs of galaxies in the three cluster regions corresponding to high- (black), intermediate- (red) and low-density (blue) environments. Continuous lines represent the best fit. The counts are per half magnitudes.

Figs. 8 and 9). Also the bright-end LF is inconsistent at more than 3σ c.l. in both bands, indicating that also the bright galaxy populations in the SSC depend on the environment. We note that the shape of the LFs vary dramatically from high- to low-density regions in both bands (see Fig. 10 for a direct comparison), demonstrating the strong effects of supercluster environment in low-density regions.

6.4 Red and blue galaxies

In order to further investigate the processes responsible for shape the galaxy LF, we divided the galaxies into red and blue according to their location with respect to the colour magnitude relation.

We determined the colour-magnitude (CM) relation by performing 100 Monte-Carlo realiza-

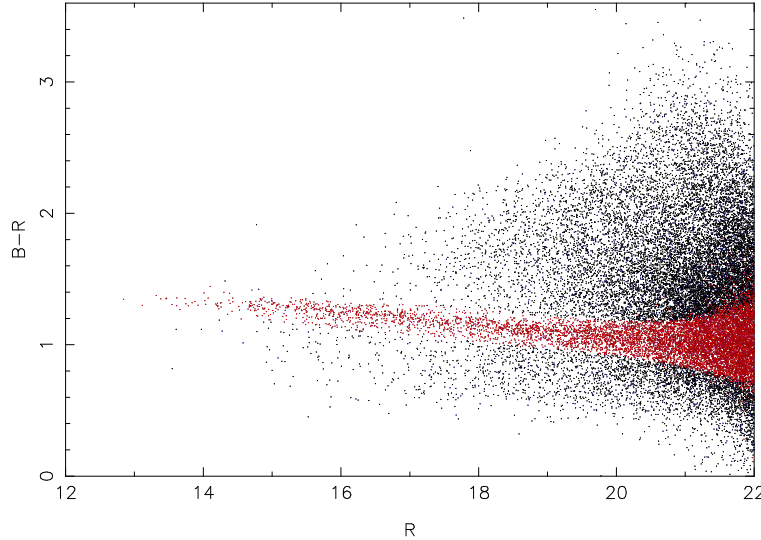


Figure 11. B-R vs R CM diagram for all the galaxies up to the completeness magnitude R=22.0 in the SOS field. Galaxies of the red sequence (see solid line) are plotted as red points.

Table 5. Fits to the LFs of blue galaxies. Errors on the M^* and α parameters are shown by the confidence contours shown in Fig. 13.

Region	m^*	M^*	α	χ^2_v	$P(\chi^2 > \chi^2_v)$
high density	16.59	-20.19	-1.39	0.78	66.1%
int density	14.66	-22.12	-1.56	0.96	48.9%
low density	14.70	-22.08	-1.52	1.05	40.0%

tions of the supercluster populations and fitting the photometric data up to R=19 by using the biweight algorithm of Beers, Flynn, & Gebhardt (1990), obtaining:

$$(B - R)_{CM} = 2.3312 - 0.0563 \times R . \quad (2)$$

We also evaluated the B-R colour dispersion around the red sequence as a function of the magnitude, $\sigma(R)$. The dispersion around the sequence is found to be consistent with the relation:

$$\sigma(R)^2 = \sigma_{int}^2 + \sigma_{(B-R)}^2(R) , \quad (3)$$

where the intrinsic dispersion σ_{int}^2 is equal to 0.0450 mag over the whole magnitude range covered (Haines et al. 2005).

In Fig. 11 the red sequence galaxies are plotted as red points. We directly compare the counts of galaxies selected on the CM relation (open circles in Fig. 7) with those derived in Sect. 6.3 (filled circles in Fig. 7) in order to exclude projection effects due to background clusters. The counts for the sequence galaxies were obtained through a statistical background subtraction, applying the same colour cut of SOS galaxies to those in the DLS control field. The distributions of red galaxies in the three different density regions are well described by the total LFs, since also in this case there is a dip at $R \sim 17.0$ ($M_R \sim -19.8$).

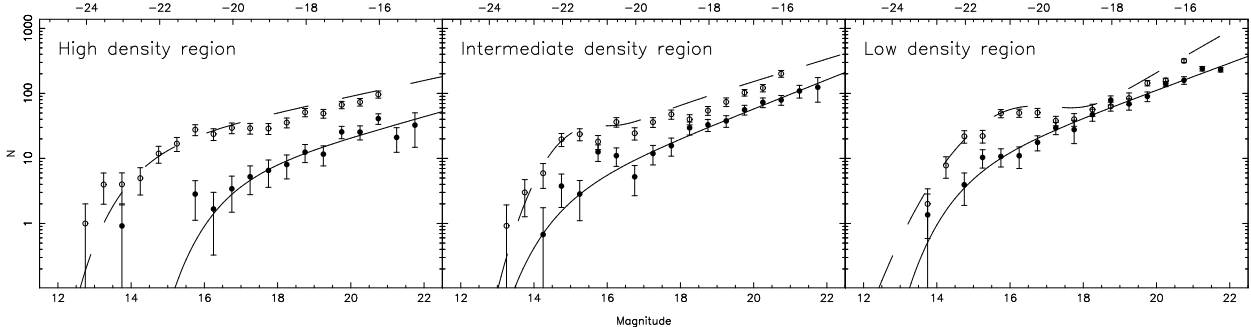


Figure 12. The R-band LFs of red (open circles) and blue galaxies (filled circles) in the three cluster regions corresponding to high-, intermediate- and low-density environments. Continuous and dashed lines represent the best fit for blue and supercluster galaxies respectively. The counts are per half magnitudes.

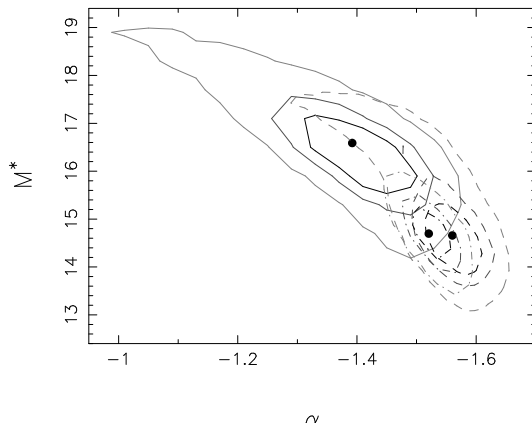


Figure 13. The 1, 2 and 3σ confidence levels for the R-band best-fitting Schechter parameters for the blue galaxies in the three cluster regions corresponding to high- (solid contours), intermediate- (dashed) and low-density (dot-dashed) environments.

We also selected the blue supercluster galaxies considering the galaxies 3σ bluer than the CM relation. Figure 12 shows the LFs obtained for the red sequence and blue galaxy population in high-, intermediate- and low-density regions. The blue galaxy LFs were obtained through a statistical background subtraction, applying the same colour cut of the supercluster galaxies to those in the DLS control fields. In contrast to the red sequence galaxies, the blue galaxy LFs are well described by a S function and do not vary with the density (see contours in Fig. 13). This indicates that the blue galaxies represent a population that have not yet interacted with the supercluster environment.

7 SUMMARY AND DISCUSSION

We have presented a detailed analysis of the LFs for galaxies in the SSC core. All the luminosity functions were calculated through a weighted parametric fit of a single Schechter function and a composite function, given by the sum of a Gaussian for the bright-end and a Schechter for the faint-end of the LF. The main results of our analysis are the following.

- The LFs in the whole SOS area have a bimodal behaviour both in B and R band. The weighted

parametric fit of a S function is unable to describe the observed LF at faint magnitudes, in particular the dips apparent at $B \sim 17.5$ ($M_B \sim -19.3$) and $R \sim 17.0$ ($M_R \sim -19.8$) and the clear upturn for galaxies fainter than 18 mag. To successfully model these dip and changes in slope a composite G+S LF is required.

- By deriving the LFs in regions with different local surface densities of $R < 21.0$ galaxies we showed that, as observed in the LFs of the whole field, a dip is present at $M_R \sim -19.8$ for LFs in intermediate- and low-density regions, while for the high-density region, the data are well represented by the S function. Moreover the faint-end slope, α , shows a strong dependence on environment, becoming steeper at $> 3\sigma$ significance level from high- ($\alpha_B = -1.46$, $\alpha_R = -1.30$) to low-density environments ($\alpha_B = -1.66$, $\alpha_R = -1.80$) in both bands.

- We derived the LFs separately for red and blue galaxy populations according to their B-R colours. The LFs of these two populations show a very different behaviour. In fact differently from the red sequence galaxy counts that are very similar to those obtained with a statistical background subtraction, the blue galaxy LFs are well described by a S function and do not vary with the density.

These results confirm and extend those of MGP94 who found a peak in the number of galaxies at $b = 18$ and suggested that the Abell function is a better representation of the integral counts than the S function. However, their optical LF is limited at galaxies three magnitudes brighter than those analysed in the present work, preventing the determination of the steepening of the LF faint-end and a more clear definition of the LF shape. On the other hand, MGP94 also noted that the CM red sequence galaxies show the broad peak at bright magnitudes in agreement with our findings.

The bimodality of the galaxy LF is commonly observed for rich clusters (e.g., Yagi et al. 2002; Mercurio et al. 2003), and using data from the RASS-SDSS galaxy cluster survey, Popesso et al. (2006) find a similar variation of the LF with environment to that observed here, but using cluster-centric radius rather than local density (e.g., Haines et al. 2004) as a proxy for environment. This observed bimodality and its variation with environment can be best accommodated in a scenario where bright and faint galaxy populations have followed different evolution histories.

The SDSS and 2dFGRS surveys have indicated that the evolution of bright galaxies is strongly dependent on environment as measured by their local density, yet is independent of the richness of the structure to which the galaxy is bound, indicating that mechanisms such as merging or suffocation play a dominant role in transforming galaxies, rather than harassment or ram pressure stripping (Gómez et al. 2003; Tanaka et al. 2004). However, it is difficult to reconcile the dramatic

deviations from the S function observed for intermediate- and low-density regions with the transformation of field galaxies being due to just merging or suffocation, neither of which should alter the shape of LF, whilst they can be explained more easily by a scenario involving mass loss of low-luminosity galaxies.

One such mechanism is galaxy harassment (Moore et al. 1996, 1998), whereby repeated close (<50 kpc) high-velocity (>1000 km s $^{-1}$) encounters with bright galaxies and the cluster's tidal field cause impulsive gravitational shocks that damage the fragile disks of late-type spirals. The cumulative effect of these shocks is the transformation of late-type spirals to spheroidal galaxies over a period of several Gyr. An important aspect of galaxy harassment is that it has virtually no effect on systems as dense as giant elliptical or spiral bulges, and hence only pure disk systems (Sc or later) are affected. While these galaxies make up the vast majority of the faint ($M > M^* + 2$) cluster galaxy population at $z \gtrsim 0.4$, they become rarer exponentially at brighter magnitudes. The encounters can drive the bulk of the dark matter and 20–75% of the stars over the tidal radius of the harassed galaxy, whereas in contrast the bulk of the gas collapses inward, and is consumed in a nuclear starburst. The combined results of these effects is a dimming of the harassed galaxy by ~ 2 magnitudes due to mass loss and passive aging of the remaining stars. These remnants are apparent in present day clusters as dwarf spheroids which often show blue cores suggesting nuclear star-formation, as well as remnant disk and bar components (Graham, Jerjen & Guzman 2003), and signs of rotational support (de Rijcke et al. 2001).

In agreement with the recent work by Popesso et al. (2006) we suggest that the observed dip at $M_R \sim -19.8$ as well as the strong dependence on environment shown by the faint-end slope in the cluster galaxy luminosity can be explained naturally as the consequence of galaxy harassment.

Alternative mechanisms such as ram-pressure stripping by the ICM or tidal stripping can effect the galaxy population only in the cluster cores, which appears inconsistent with our observation that the dip is greatest in the low-density regions 1–2 Mpc from the nearest cluster. However, given the high infall velocities, any galaxy encountering the ICM is likely to be stripped rapidly of their gas, bringing star-formation to a swift halt. Given the high infall velocities, and the typical highly eccentric orbits of cluster galaxies, the low- and intermediate-density regions are likely to contain a significant fraction of galaxies that have already encountered the dense ICM. In high-density regions, high-velocity dispersions inhibit merging processes (e.g., Mihos 2004), hence it is unlikely that dwarf galaxies merge to produce bigger galaxies at the cluster centres. The most likely explanation for the lack of dwarf galaxies near the centre is tidal or collisional disruption of the dwarf galaxies.

This interpretation is also confirmed when analysing separately red sequence galaxies. In fact the red galaxy counts exhibit a behaviour similar to those of the LFs obtained with a statistical background subtraction, confirming the excess of dwarf early type galaxies. Moreover, differently from red sequence galaxies, the blue galaxy LFs are well described by a S function with a slope $\alpha \sim -1.50$ and do not vary with density. This slope is consistent with those recently derived by Blanton et al. (2005) and Madgwick et al. (2002) for field SDSS and 2dF galaxies respectively. This suggest that the observed blue galaxy population is characterized by infalling galaxies that have not yet interacted with the super cluster environment and transformed by the harassment mechanism.

In a forthcoming paper (Haines et al. 2005) we will investigate in detail the distribution of red and blue galaxies in the SSC environment.

ACKNOWLEDGMENTS

We thank the Deep Lens Survey and NOAO, who provided the galaxy counts used to derive the LFs. We thank the anonymous referee for useful comments. AM is supported by the Regione Campania (L.R. 05/02) project ‘*Evolution of Normal and Active Galaxies*’ and by the Italian Ministry of Education, University, and Research (MIUR) grant COFIN2004020323: *The Evolution of Stellar Systems: a Fundamental Step towards the Scientific Exploitation of VST*. CPH, AG and NK acknowledge the financial supports provided through the European Community’s Human Potential Program, under contract HPRN-CT-2002-0031 SISCO. NK and GC are partially supported by the Italian Ministry of Education, University, and Research (MIUR) grant COFIN2003020150: *Evolution of Galaxies and Cosmic Structures after the Dark Age: Observational Study* and grant COFIN200420323: *The Evolution of Stellar Systems: a Fundamental Step towards the Scientific Exploitation of VST*, respectively.

REFERENCES

- Abell G. O., Corwin H. G. Jr., Olowin R. P., 1989, ApJS, 70, 1
- Arnouts S., de Lapparent V., Mathez G., et al., 1997, A&AS, 124, 163
- Balogh M. L., Navarro J. F., Morris S. L., 2000, ApJ, 540, 113
- Bardelli S., Zucca E., Malizia A., et al., 1996, A&A, 305, 435
- Bardelli S., Zucca E., Zamorani G., Moscardini L., Scaramella R., 2000, MNRAS, 312, 540
- Bardelli S., Zucca E., Baldi A., 2001, MNRAS, 320, 387

Beers T.C., Flynn K., Gebhardt K., 1990, AJ, 100, 32

Bernstein G. M., Nichol R. C., Tyson J. A., Ulmer M. P., Wittman D., 1995, AJ, 110, 1507

Bertin E., Arnouts S., 1996, A&AS, 331, 439

Biviano A., Durret F., Gerbal D., et al., 1995, A&A, 297, 610

Blanton M. R., Lupton R. H., Schlegel D. J., et al., 2005, ApJ, 631, 208

Bower R. G., Lucey J. R., Ellis R. S., 1992, MNRAS, 254, 589

Bruzual G., Charlot S., 2003, MNRAS, 344, 1000

Butcher H., Oemler A. J., 1984, ApJ, 285, 426

De Filippis E., Schindler S., Erben T., 2005, A&A, 444, 387

de Lapparent V., Galaz G., Bardelli S., Arnouts S., 2003, A&A, 404, 831

de Lapparent V., 2003, A&A, 408, 845

De Rijcke S., Dejonghe H., Zeilinger W. W., Hau, G. K. T., 2001, ApJ, 559, 21

Diaferio A., Kauffmann G., Balogh M. L., et al., 2001, MNRAS, 323, 999

Drake N., Merrifield M. R., Sakelliou I., Pinkney J. C., 2000, MNRAS, 314, 768

Dressler A., Oemler A. J., Butcher H. R., Gunn J., 1994, ApJ, 430, 107

Drinkwater M. J., Parker Q. A., Proust D., Slezak E., Quintana H., 2004, PASA, 21, 89

Finoguenov A., Henriksen M. J., Briel U. G., de Plaa J., Kaastra J. S., 2004, ApJ, 611, 811

Fujita Y., 1998, ApJ, 509, 587

Garilli B., Maccagni D., Andreon S., 1999, A&A, 342, 408

Ghigna S., Moore B., Governato F., et al., 1998, MNRAS, 300, 146

Gómez P. L., Nichol R. C., Miller C. J., et al., 2003, ApJ, 584, 210

Graham A. W., Jerjen H., Guzman R., 2003, AJ, 126, 1787

Haines C. P., Mercurio A., Merluzzi P., et al, 2004, A&A, 425, 783

Haines C. P., Merluzzi P., Mercurio, A., et al, 2005, MNRAS, submitted

Hambly N. C., MacGilivray H. T., Read M. A., 2001, MNRAS, 326, 1279

Kang X., Jing Y. P., Mo H. J., Börner, 2005, ApJ, 631, 21

Kron R. G., 1980, ApJS, 43, 305

Kull A., Böhringer H., 1999, A&A, 341, 23

Landolt A. U., 1992, AJ, 104, 340

Larson R. B., Tinsley B. M., Caldwell C. N., 1980, ApJ, 237, 692

Madgwick D. S., Lahav O., Baldry I. K., et al., 2002, MNRAS, 333, 133

Melnick J., Quintana H., 1981, A&AS, 44, 87

Mercurio A., Massarotti M., Merluzzi P., et al., 2003, A&A, 408, 57

Metcalfe N., Godwin J. G., Spenser S. D., 1987, MNRAS, 225, 581

Metcalfe N., Godwin J. G., Peach J. V., 1994, MNRAS, 267, 431 (MGP94)

Mihos J. C., 2004, in *Clusters of Galaxies: Probes of Cosmological Structure and Galaxy Evolution*, Cambridge University Press, edited by J.S. Mulchaey, A. Dressler, and A. Oemler, p. 278

Miller N. A., 2005, AJ, 130, 2541

Moore B., Katz N., Lake G., Dressler A., Oelmer A., 1996, Nat, 379, 613

Moore B., Lake G., Katz N., 1998, ApJ, 495, 139

Molinari E., Chincarini G., Moretti A., De Grandi S., 1998, A&A, 338, 874

Pisani A., 1993, MNRAS, 265, 706

Pisani A., 1996, MNRAS, 278, 697

Popesso P., Biviano A., Böhringer H., Romaniello M., 2006, A&A, 445, 29

Quintana H., Carrasco E. R., Reisenegger A., 2000, AJ, 120, 511

Raychaudhury S., 1989, Nature, 342, 251

Reisenegger A., Quintana H., Carrasco E. R., Maze J., 2000, AJ, 120, 523

Rines K., Geller M. J., Kurtz M. J., Diaferio A., 2005, AJ, 130, 1482

Schechter P., 1976, ApJ, 203, 297

Schlegel D. J., Finkbeiner D. P., Davis M., 1998, ApJ, 500, 525

Shapley H., 1930, Bull. Harvard Obs., 874, 9

Smith G. P., Treu T., Ellis R. S., Moran S. M., Dressler A., 2005, ApJ, 620, 78

Springel V., White S.D. M., Tormen G., Kauffmann G., 2001, MNRAS, 328, 726

Struble M. F., M., Rood H. J., 1999, ApJS, 125, 35

Tanaka M., Goto T., Okamura S., Shimasaku K., Brinkmann J., 2004, AJ, 128, 2677

Tanaka M., Kodama T., Arimoto N. et al., 2005, MNRAS, 362, 268

Treu T., Ellis R. S., Kneib J. P., et al., 2003, ApJ, 591, 53

Vandame B., 2004, PhD thesis

Venturi T., Bardelli S., Morganti R., Hunstead R. W., 2000, MNRAS, 314, 594

Venturi T., Bardelli S., Dallacasa D., et al., 2003, A&A, 402, 913

Wittman D. M., Tyson J. A., Dell'Antonio I. P., et al., 2002, SPIE, 4836, 73

Wolf C., Meisenheimer K., Kleinheinrich M., et al., 2004, A&A, 421, 913

Yagi, M., Kashikawa, N., Sekiguchi, M., et al., 2002, AJ, 123, 87